A CASE STUDY OF MACROPARTICAL REDUCING WHILE COATING TIALCN BY ARC CATHODE USING PERMANENT MAGNET

Nguyen Duc Luan[1], Pham Duc Cuong[1,*]

DOI: http://doi.org/ 10.57001/huih5804.2025.239

ABSTRACT

This study aimed to investigate the effect of using a permanent magnet to increase the ratio of plasma and particles in arc source deposition. A permanent magnet was installed after surface the arc source to create a magnetic field that would control the plasma arc and reduce the formation of macro particles. The size and strength of the magnet were carefully chosen to ensure that the magnetic field was strong enough to generate the desired effect on the plasma arc. The results showed that the use of a permanent magnet significantly increased the ratio of plasma and particles in arc source deposition. The magnetic field created by the permanent magnet effectively controlled the plasma arc and reduced the formation of macro particles, resulting in a higher percentage of plasma in the deposition process. This improvement in the plasma-to-particle ratio led to higher-quality thin films, with fewer defects and higher uniformity. The study also found that the magnetic field strength and distance position of the permanent magnet could be adjusted to optimize the plasma-to-particle ratio for specific deposition applications with a distance from the permanent magnet to the target surface is 0 -15mm. The validity of this was confirmed by maintaining the coating parameters constant and depositing TiAlCN on SKD11 steel. The effectiveness of the reduction of microparticles was examined by microscopy. The only variables that were altered were the distance between the permanent magnet and the back of the target, as well as the shape of the target surface after a duration of 2 hours.

Keywords: *Arc cathode; Filtered arc; Permanent magnet.*

[1]HaUI Institute of Technology, Haaoi University Industry, Vietnam

[*]Email: phamcuong@haui.edu.vn

Received: 18/2/2025

Revised: 10/5/2025

Accepted: 25/7/2025

1. INTRODUCTION

Arc source deposition is widely used for depositing thin films in various industries, including aerospace, electronics, and biomedical engineering. However, the deposition process often results in the formation of macro particles, affecting the quality and uniformity of the deposited thin films. One method to reduce the formation of macro particles is by controlling the plasma arc in the deposition process using a magnetic field generated by a permanent magnet.

The size of macroparticles (MPs) is commonly stated to be between 0.1 and 10m, though the limitations of the diagnostic technique used usually specify this lower limit. As a result, tinier particles known as "nanoparticles" may be present in the plasma [1]. For this paper, the term 'particle' refers to macroparticles, microparticles, nanoparticles, and droplets in a broad sense.

Particle filters are commonly used in cathodic arc plasma systems to reduce deposition substrate contamination. The plasma transport efficiency of these filters is defined as the ratio of ions leaving the filter to those entering it. However, calculating the ion flow into the filter can be difficult, so the filtered ion current standardized by the arc current is a more precise value. The system coefficient, denoted as k = Ii, filtered/Iarc, represents this value and characterizes the entire linked system of the arc source and filter.

Although the filter can theoretically transport plasma up to 100%, it typically has only a few per cent system coefficient since electrons are responsible for most of the arc current. The system coefficient can never reach 100% because most of the arc current is electrons.

Fig. 1. Plasma recreation of particles in areas of the cathode that have liquid

Cathodic arcs produce a concentrated current known as cathode spots [2]. Spots like these are critical for generating plasma, emitting electrons, and transmitting

currents between the cathode and anode. During cathode spots, particles are formed when plasma interacts with solid material [3]. Cathode spots are formed by plasma pressure acting on molten cathode material, as described in Juttner's cathode spot model (Fig. 1).

When the cathode points are not constant, particle production occurs, which cannot be avoided unless the arc operates in another cathode mode [4, 5]. Spotless vapor is a mode of operation that uses a material with a high vapor pressure at a high temperature. At the same time, an arc cathode is a mode that uses an evaporating anode [6-11].

Researchers have been studying the effect of magnetic fields on a range of materials [12-14]. It has been seen that these fields can obstruct the development of scale in water by altering the carbonate structure in the fluid. Moreover, the potential impacts of magnetic fields from mobile phones and electric power lines on living creatures have also been investigated. With the growth of technology, the utilization of magnets has significantly risen, including electric motors, generators, and data storage. However, little information is accessible in the literature regarding the magnetic fields created by these magnets, and analytical expressions are hard to come by. Generally, numerical techniques such as the finite-element method are used to calculate these fields [15, 16]. Recently, the field of circular magnets has been discussed, and this paper endeavours to develop an alternate method for computing the area made by a permanent magnet [17, 18].

In a specific deposition configuration, Andersson et al. demonstrated that the magnetic field applied to direct the arc on the cathode surface has a notable effect on the ionization degree of the plasma and the confinement of highly energetic electrons in front of the cathode [19].

This study aimed to examine the effect of using permanent magnets on reducing the microparticle number in arc source deposition.

2. MATERIALS AND METHODS

2.1. Theoritical

The magnetic field of a permanent magnet is calculated by calculating its vector potential using the formula $\vec{B} = \Delta \times \vec{A}$. If the magnetization of a body remains constant within its volume, but changes to zero outside of it, such as in the case of a magnet, the potential at a specific point can be represented as a surface integral, as described in reference [19].

$$\vec{A}(\vec{x}) = \frac{\mu_0}{4\pi} \oint \frac{\vec{M}\left(\vec{x'}\right) \times \hat{n'}}{\left|\vec{x'} - \vec{x}\right|} \quad (1)$$

Where $\vec{M}$ is the magnetization per unit volume of the magnet, $\hat{n'}$ is the unit vector perpendicular to the surface at a point $\vec{x'}$ and μ_0 is the vacuum magnetic susceptibility. We consider the magnet as a continuous distribution of dipoles that occupy a volume dV and possess a magnetic dipole moment $d\vec{m} = \vec{M}dV$. We assume that the magnetization is constant inside the volume and remains unaffected by any external magnetic field, meaning that the magnet is assumed to be hard. For simplicity, we always choose $\vec{M} = M\hat{k}$. To make the calculations simpler, we begin by remembering that the magnetic scalar potential and induction field generated by a magnetic dipole situated at the origin at a point $\vec{x'}$ are expressed as:

$$\Phi_{dipole}(\vec{x}) = \frac{1}{4\pi} \frac{\vec{m} \cdot \hat{n}}{\left|\vec{x}\right|^2} \quad (2)$$

$$\vec{B}_{dipole}(\vec{x}) = \frac{\mu_0}{4\pi} \frac{3\hat{n}\left(\hat{n} \cdot \vec{m}\right) - \vec{m}}{\left|\vec{x}\right|^3} \quad (3)$$

Where $\vec{m}$ is the moment of a magnetic dipole.

Magnets' magnetic fields are calculated by integrating the contributions of the infinitesimal dipoles of their scalar potentials or fields over the volume of their mass $\vec{B} = -\mu_0 \nabla \Phi$. In many cases, configurations that possess azimuthal symmetry provide useful mathematical properties, regardless of the method used. Typically, the symmetry axis is the z-axis, and the scalar potential on the axis can be calculated relatively simply, with this function being used to determine the solution off-axis. A solenoid's magnetic field has been calculated previously using successive derivatives of the axial function, for example by Jackson [20]. Laplace equation solutions have a property that is used in this work. When the solution on the symmetry axis is expressed as a series, this property can prove useful in electrostatic potential cases [15, 19].

$$\Phi_{axis}(z) = \sum_{\ell=0}^{\infty} \left(U_\ell z^\ell + \frac{V_\ell}{z^{\ell+1}} \right) \quad (4)$$

then the solution at any point in space (r, θ) is given by:

$$\Phi(r,\theta) = \sum_{\ell=0}^{\infty} \left(U_\ell r^\ell + \frac{V_\ell}{r^{\ell+1}} \right) P_\ell(\cos\theta) \quad (5)$$

where $P_\ell(\cos\theta)$ is the Legendre polynomial of order. Therefore, all we have to do is to calculate $\Phi_{axis}(z)$ and expand it in powers of z.

Now, we illustrate this approach with the case of a cylinder magnet.

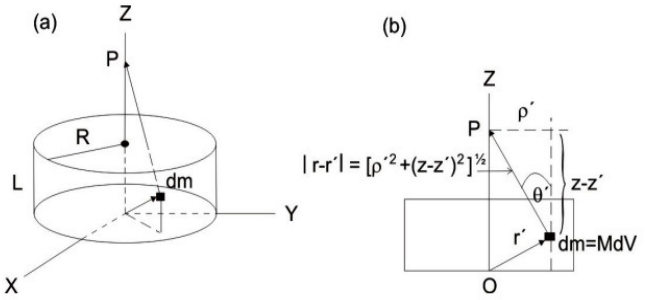

Fig. 2. (a) diagram representing a cylindrical magnet; (b) method for computing the magnetic field generated by the magnet

As shown in Fig. 2 (b), the potential on the z axis due to each infinitesimal dipole is given by:

$$d\Phi_{axis}=\frac{1}{4\pi}dm\frac{\cos\theta'}{\left|\vec{r}-\vec{r}'\right|^2}=\frac{1}{4\pi}MdV\frac{z-z'}{\left|\vec{r}-\vec{r}'\right|^3}$$
$$=\frac{M}{4\pi}\frac{z-z'}{\left[\left(z-z'\right)^2+\rho'^2\right]^{3/2}}\rho'd\rho'dz'd' \quad (6)$$

Therefore, the sum of the scalar potentials along the axis can be expressed as:

$$\Phi_{axiz}(z)=\frac{M}{4\pi}\int\frac{z-z'}{\left[\left(z-z'\right)^2+\rho'^2\right]^{3/2}}\rho'd\rho'dz'd'$$
$$=\frac{M}{2}\int_0^L(z-z')dz'\int_0^R\frac{\rho'd\rho'}{\left[\left(z-z'\right)^2+\rho'^2\right]^{3/2}} \quad (7)$$

$$=\frac{M}{2}\int_0^L(z-z')dz'\left(-\frac{1}{\sqrt{\left(z-z'\right)^2+\rho'^2}}\Big|_{\rho'=0}^{\rho'=R}\right) \quad (8)$$
$$=\frac{M}{2}\sqrt{\left(z-z'\right)^2+\rho'^2}\Big|_{z'=0}^{z'=L}\Big|_{\rho'=0}^{\rho'=R}$$

The resulting scalar potential can be simplified by ignoring any additive constants.

$$\Phi_{axiz}(z)=\frac{M}{2}\sqrt{(z-L)^2+R^2}-\sqrt{z^2+R^2} \quad (9)$$

The field on the z-axis is then given by

$$B(z)=\frac{\mu_0 M}{2}\left(\frac{z}{\sqrt{z^2+R^2}}-\frac{z-L}{\sqrt{(z-L)^2+R^2}}\right) \quad (10)$$

2.2. Experimental

TiAlCN coatings are created by the cathodic arc technique of PVD method in a vacuum environment, capable of creating coatings with high adhesion and hardness thanks to the strong plasma energy source and high ion density. The coating process is carried out on the HCM-700 coating system (Fig. 3) with an integrated sample heater, automatic gas flow control and cathode pulse source. HCM-700 is a semi-industrial PVD coating equipment that has been researched, manufactured and integrated, with the ability to use separately or simultaneously 2 sputtering and cathode arc techniques in one coating process. The basic parameters are as follows:Arc source power: 10kW, bias source power: 20kW, maximum vacuum: 5×10^{-4}Pa, maximum heating temperature: 500^0C

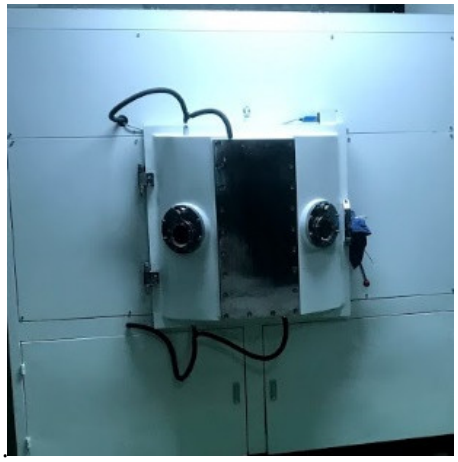

(a)

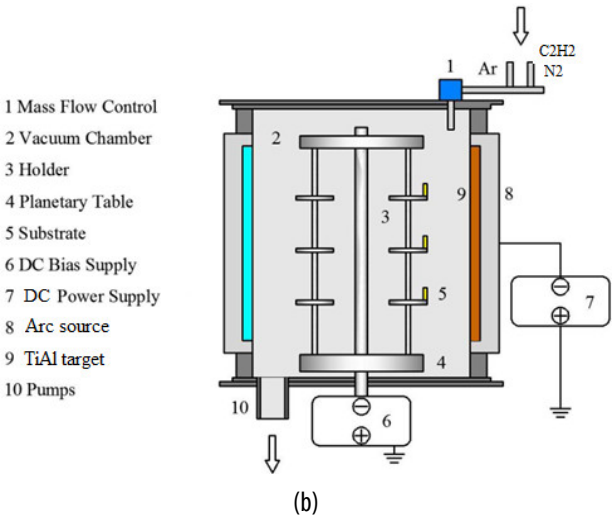

(b)

Fig. 3. (a) The coating machine HCM-700 and (b) schematic of the arc cathode deposition

The SKD61 was chosen as substrates cut into pieces of φ 20 × 5mm by wire cutting. The SKD61 samples were

then mirrored and polished to avoid the change in the microstructure of the alloy substrate due to the heat effect zone caused by the wire-cutting process. The SKD61 samples were polished and cleaned in an ultrasonic bath containing acetone, methanol, and deionized water before drying with nitrogen gas. A base pressure of 5×10^{-3}Pa was achieved using a turbo-molecular pump and rotary pump before introducing gases. The sample holder was heated to 450°C during deposition once a high vacuum of at least 5×10^{-3}Pa was reached. The targets were etched and cleaned using argon for 5 minutes with a fixture rotation of 6rpm.

Table 1. Parameters and fabrication process of TiAlCN coating

No	Step	Time (min)	Temperature (°C)	Arc current (A)	Bias Voltage (V)	Pressure (Pa)
1	Cleaning	5	450	-	-900	1.2×10^{0}
2	Coating TiAl	5	450	80	-900	5×10^{-3}
3	CoatingTiAlCN	10	450	80	-650	5×10^{-1}
4	CoaingTiAlCN	90	450	80	-100	5×10^{-1}
5	Cooling down	80	<150	-	-	-

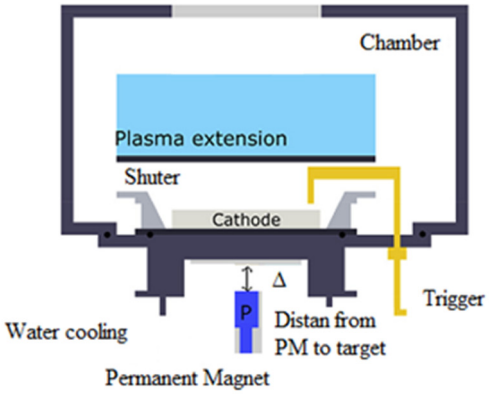

Fig. 4. The schematic graph of the vacuum cathodic arc presents the permanent magnet

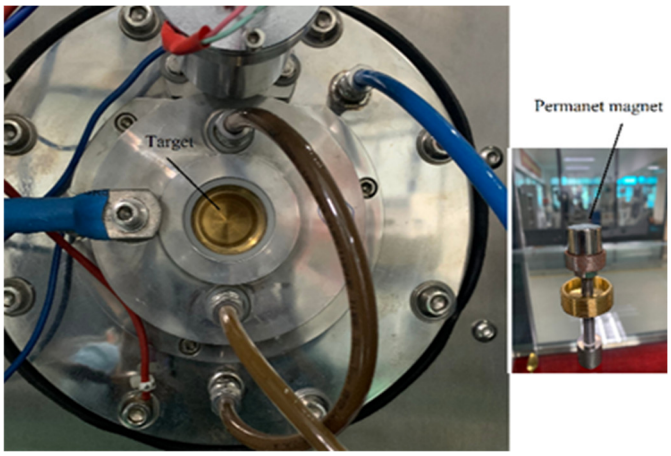

Fig. 5. The cathode arc source and permanent magnet

To control the movement of cathode spots, the magnetic system used a permanent magnet cylinder (shown in Fig. 4). This magnet was placed outside the grounded vacuum chamber behind each arc source. By adjusting the distance between the magnet and the target in increments of 1mm from 0 - 15mm, the strength of the generated magnetic field could be varied to produce different configurations. The permanent magnet measured 12 × 20mm (shown in Fig. 5).

3. RESULTS AND DISCUSSION

3.1. Results

According to the results, the magnetic flux intensity decreases from near too far from the cathode, exhibiting an axisymmetric distribution. An acute angle is formed between the magnetic flux and the target surface at the edge of the cathode. A magnetic flux guide increases the transverse magnetic component by focusing and enhancing the magnetic flux. A transverse and normal component of different magnetic flux densities on the cathodic target surface were measured, and the transverse component increased with increasing target distance while the normal component decreased. A change in distance between the permanent magnet and arc source surface increased the transverse magnetic flux density from 46G to 95G at the bottom of the inclined wall shoulder.

With increasing magnetic field intensity, MPs (microparticles) density and size decrease in TiAlCN films, as discussed in the article. SEM micrographs show that weak AMF results in mostly large liquid particles, while strong AMF results in mostly small, solidified particles.

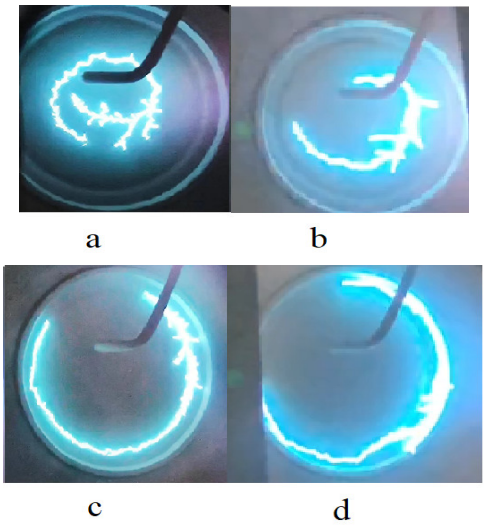

Fig. 6. A schematic illustration and a series of static images of the motion of cathode spots under different magnetic field intensities:

(a): Δ = 15mm,(b): Δ = 10mm,(c): Δ = 5mm,(a): Δ = 0mm

The number of MPs classified by their diameters also decreases with the transverse magnetic field, indicating a fractal characteristic of MPs distribution on films, as shown in Fig. 6 (a). As the AMF intensity increases, the cathode spot tends to refine, rotate, and drift toward the cathode target's edge. According to Fig. 6(b), this image changes from a bright, large cathode spot pattern to a thin, elongated line. When exposed to a high AMF, the cathode spot shifts towards the cathode surface and follows a circular trajectory. On the cathode surface, a new cathode spot is ignited, split, and extinguished several times, as shown in Fig. 6(c).

Fig. 7 shows the investigated coatings identified as A to D according to the applied distance from the permanent magnet to the target surface. Increasing the distance permanent magnet from 0mm (coating A) to 15mm (coating D) causes an increase in coating thickness from 1.82µm (coating A) to 2.20µm (coating D).

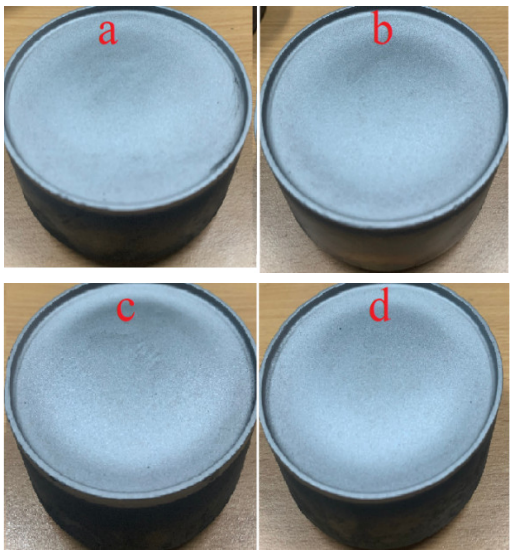

Fig.7. Dimension of cathode spots motion under different magnetic fields: (a): Δ = 0mm,(b): Δ = 5mm,(c): Δ = 10mm,(a): Δ = 15mm

Table 2. Investigated coatings and their respective distance from permanent magnet to target, coating thickness

No	Simple	Distance (D mm)	Thickness (µm)	Diameter cathode spots motion (mm)
1	A	0	1.82	71.5
2	B	5	1.91	68.1
3	C	10	1.99	64.9
4	D	15	2.20	59.8

SEM micrographs in Fig. 8 illustrate the surface morphology of coatings A(a), B(b), C(c), and D(d) under a microscope. The coatings display similar amounts of droplets and densified structures that arise from the bombardment of ion flux. Coating A (a) has a smoother surface than coatings B(b), C(c), and D (d).

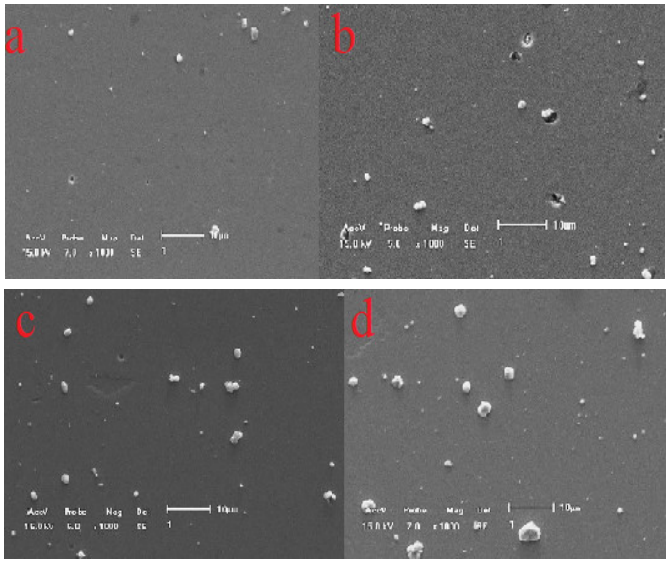

Fig. 8. SEM micrographs of the MPs on the TiAlCN film surfaces with different distance (a): Δ = 0mm,(b): Δ = 5mm,(c): Δ = 10mm,(a): Δ = 15mm

3.2. Discussion

The deposition flux produced in a cathodic vacuum arc is characterized by a high degree of ionization, consisting predominantly of electrons (approximately 90% of the total arc current) and a smaller fraction of ions (around 10%). Because electrons have significantly lower mass compared to ions or other charged species present in the plasma, they are much more susceptible to magnetic field influences. This sensitivity allows external magnetic fields to play a substantial role in modifying the behavior of the plasma within the arc discharge system.

Experimental observations have shown that the motion of cathode spots during vacuum arc deposition is inherently stochastic and is governed by multiple interacting factors, including geometric enhancement effects at the cathode surface and inherent plasma instabilities. When an external magnetic field is applied to the cathode, three characteristic components of cathode spot motion are typically observed: (i) a random walk, associated with stochastic fluctuations; (ii) retrograde motion, where the spot moves opposite to the local current density vector; and (iii) Robson drift, a steady drift motion caused by the applied magnetic field and plasma interaction.

At sufficiently high magnetic field strengths, cathode spot motion exhibits complex rotational and drift

behaviors. In particular, chrysanthemum-like structures on the cathode surface were observed, which formed when the cathode spot rotated and drifted toward the edge of the target as the magnetic field intensity increased. This behavior indicates that the magnetic field exerts a strong influence on the plasma sheath and cathode spot dynamics. Moreover, due to the incorporation of an inclined shoulder along the wall of the cathode assembly, the magnetic field could not entirely prevent the cathode spot from remaining attached to the cathode surface, even under conditions of relatively strong applied fields.

During the explosive nature of cathode spot activity, molten cathode material is ejected, giving rise to the generation of macroparticles, which are often undesired in high-quality coating processes. Detailed observations revealed that luminous group spots (GSs), which represent concentrated plasma emission regions, exhibited distinct trajectory patterns near the center of the cathode surface as the magnetic field strength increased. Furthermore, as the threshold magnetic field strength was elevated beyond a critical value, these trajectories expanded significantly, indicating enhanced cathode spot mobility and redistribution over a larger surface area.

These findings underscore the complexity of cathode spot behavior under magnetic field control and highlight the intricate interplay between plasma dynamics, magnetic confinement, and macroparticle generation, which are critical factors in optimizing vacuum arc deposition processes for high-performance coatings.

4. CONCLUSION REMARKS

In this study, a novel method is proposed for calculating the magnetic field generated by a permanent magnet with azimuthal symmetry at arbitrary spatial locations. The configuration and spacing of the permanent magnets were optimized to control the position and size distribution of cathode spots in metal vapor cathodic vacuum arc discharges. Based on the available data, the application of permanent magnets for macroparticle mitigation during TiAlCN coating deposition via arc cathode technology represents a promising advancement in coating science. The incorporation of permanent magnets has demonstrated effectiveness in reducing both the size and quantity of macroparticles, thereby enhancing the overall quality and functional performance of the deposited coatings.

ACKNOWLEDGEMENTS

This work was carried out with in the framework of the project "Research on fabricate TiAlCN coating on steel substrate for application in coating cutting tools used in high-speed milling", code HD 48-2024-RD/HĐ-ĐHCN.

REFERENCES

[1]. Y. Xu, Y. Liu, X. Li, W. Chen, J. Lin, "Macroparticle reduction and surface improvement of cathodic arc deposited coatings via magnetic filter optimization," *Surface and Coatings Technology*, 420, 127307, 2021. doi: 10.1016/j.surfcoat.2021.127307.

[2]. S. J. Bull, J. Lin, "Advances in arc evaporated coating processes: controlling macroparticles and film growth," *Vacuum*, 192, 110430, 2021. doi: 10.1016/j.vacuum.2021.110430.

[3]. C. Guo, H. Li, Z. Wang, "Influence of substrate bias on macroparticle generation in cathodic arc evaporation," *Surface and Coatings Technology*, 410, 126955, 2021. doi: 10.1016/j.surfcoat.2021.126955.

[4]. M. Bobzin, E. Lugscheider, R. Cremer, "Arc evaporation processes with advanced cathode spot control for reduced droplet formation," *Coatings*, 11, 3, 314, 2021. doi: 10.3390/coatings11030314.

[5]. D. Jiang, F. Wang, H. Zhang, "Surface properties of TiAlN coatings deposited by cathodic arc evaporation with magnetic field steering," *Thin Solid Films*, 723, 138584, 2021. doi: 10.1016/j.tsf.2021.138584.

[6]. J. Andersson, J. Sjölén, M. Johansson, "Effect of deposition energy on the microstructure of TiAlN arc evaporated coatings," *Surface and Coatings Technology*, 412, 126946, 2021. doi: 10.1016/j.surfcoat.2021.126946.

[7]. Y. Zhang, L. Xie, H. Liu, "Numerical modeling of cathode spot dynamics in vacuum arc discharges," *Plasma Sources Science and Technology*, 30, 8, 085006, 2021. doi: 10.1088/1361-6595/ac12a5.

[8]. H. Lee, S. J. Park, "Macroparticle filtering and film property optimization in cathodic arc PVD systems," *Journal of Vacuum Science & Technology A*, 39, 4, 043201, 2021. doi: 10.1116/6.0001023.

[9]. K. H. Kim, J. H. Kim, S. W. Park, "TiAlN coating deposited by filtered cathodic arc for cutting tool applications," *Coatings*, 11, 5, 515, 2021. doi: 10.3390/coatings11050515.

[10]. S. Nayak, T. W. Hsu, L. Rogström, M. Moreno, J. M. Andersson, M. P. Johansson-Jõesaar, "In-situ real-time evolution of intrinsic stresses during growth of cathodic arc deposited (Al,Ti)N coatings," *arXiv preprint*, 2023. [Online]. Available: https://arxiv.org/abs/2301.03935

[11]. P. E. Lee, Y. K. Tu, M. H. Tsai, C. W. Tsai, J. W. Yeh, "Macroparticle reduction and its transport mechanism through a magnetic filter during cathodic vacuum arc deposition with an HEA target," *Coatings*, 12, 10, 1437, 2022. doi: 10.3390/coatings12101437.

[12]. K. Zhang, W. Lang, H. Wang, "Study on microspot splitting characteristics in cathode spot motion of vacuum arc," *Vacuum*, 205, 111462, 2023. doi: 10.1016/j.vacuum.2022.111462.

[13]. R. K. Ghadai, K. Kamaraj, A. Kumar, "The effect of cathode arc current on the structures of TiN thin films prepared by cathodic arc deposition," *Materials*, 16, 2, 512, 2023. doi: 10.3390/ma16020512.

[14]. D. L. Chen, Y. F. Wu, X. B. Tian, "Simulation of plasma flow and macroparticle transport in vacuum arc plasma sources," *IEEE Transactions on Plasma Science*, 49, 6, 1948-1955, 2021. doi: 10.1109/TPS.2021.3073135.

[15]. F. Wang, Z. Xu, L. Zheng, "Cathodic arc plasma characteristics with composite cathodes for hard coating deposition," *Surface and Coatings Technology*, 431, 128012, 2022. doi: 10.1016/j.surfcoat.2021.128012.

[16]. C. P. Chen, M. Andersson, "High-rate deposition of TiAlCN coatings by cathodic arc with macroparticle control," *Thin Solid Films*, 735, 138883, 2021. doi: 10.1016/j.tsf.2021.138883.

[17]. J. S. Li, W. Q. Xu, H. L. Xie, "Tribological behavior of TiAlN coatings prepared by cathodic arc with different bias voltages," *Tribology International*, 168, 107427, 2022. doi: 10.1016/j.triboint.2022.107427.

[18]. S. Y. Lee, H. M. Park, J. S. Kim, "Cathode spot motion and macroparticle emission in vacuum arc discharges: experimental and modeling studies," *Plasma Chemistry and Plasma Processing*, 42, 521-538, 2022. doi: 10.1007/s11090-021-10141-y.

[19]. E. Martínez, P. M. Romero, G. García, "Filtered cathodic vacuum arc deposition of nanostructured hard coatings: trends and challenges," *Coatings*, 12, 8, 1121, 2022. doi: 10.3390/coatings12081121.

[20]. H. B. Kim, S. Y. Kang, C. S. Park, "Numerical simulation of electromagnetic fields in filtered arc sources for macroparticle control," *IEEE Transactions on Magnetics*, 59, 1, 4600105, 2023. doi: 10.1109/TMAG.2022.3214567.